CrossMark
click for updates

Electron Accepting Units of the Diheme Cytochrome c TsdA, a Bifunctional Thiosulfate Dehydrogenase/Tetrathionate Reductase*◆

Julia M. Kurth[‡1,2], José A. Brito[§1,3], Jula Reuter[‡4], Alexander Flegler[‡], Tobias Koch[‡], Thomas Franke[‡], Eva-Maria Klein[‡5], Sam F. Rowe[¶6], Julea N. Butt[¶7], Kevin Denkmann[‡8], Inês A. C. Pereira[§], Margarida Archer[§9], and Christiane Dahl[‡10]

From the ‡Institut für Mikrobiologie & Biotechnologie, Rheinische Friedrich-Wilhelms-Universität Bonn, 53115 Bonn, Germany, the §Instituto de Tecnologia Química e Biológica António Xavier, Universidade Nova de Lisboa (ITQB-UNL), 2780-157 Oeiras, Portugal, and the ¶Centre for Molecular and Structural Biochemistry, School of Chemistry and School of Biological Sciences, University of East Anglia, Norwich Research Park, Norwich NR4 7TJ, United Kingdom

Edited by Ruma Banerjee

The enzymes of the thiosulfate dehydrogenase (TsdA) family are wide-spread diheme c-type cytochromes. Here, redox carriers were studied mediating the flow of electrons arising from thiosulfate oxidation into respiratory or photosynthetic electron chains. In a number of organisms, including *Thiomonas intermedia* and *Sideroxydans lithotrophicus*, the *tsdA* gene is immediately preceded by *tsdB* encoding for another diheme cytochrome. Spectrophotometric experiments in combination with enzymatic assays in solution showed that TsdB acts as an effective electron acceptor of TsdA *in vitro* when TsdA and TsdB originate from the same source organism. Although TsdA covers a range from −300 to +150 mV, TsdB is redox active between −100 and +300 mV, thus enabling electron transfer between these hemoproteins. The three-dimensional structure of the TsdB-TsdA fusion protein from the purple sulfur bacterium *Marichromatium purpuratum* was solved by X-ray crystallography to 2.75 Å resolution providing insights into internal electron transfer. In the oxidized state, this tetraheme cytochrome c contains three hemes with axial His/Met ligation, whereas heme 3 exhibits the His/Cys coordination typical for TsdA active sites. Interestingly, thiosulfate is covalently bound to Cys[330] on heme 3. In several bacteria, including *Allochromatium vinosum*, TsdB is not present, precluding a general and essential role for electron flow. Both *Av*TsdA and the *Mp*TsdBA fusion react efficiently *in vitro* with high potential iron-sulfur protein from *A. vinosum* (E_m +350 mV). High potential iron-sulfur protein not only acts as direct electron donor to the reaction center in anoxygenic phototrophs but can also be involved in aerobic respiratory chains.

The bifunctional thiosulfate dehydrogenase/tetrathionate reductase TsdA is present in various organisms of different proteobacterial genera (1). In the diheme cytochrome c from the purple sulfur bacterium *Allochromatium vinosum*, an axial histidine/cysteine ligation of the central iron atom has been firmly established for the active site heme (2). This type of ligation is rare among prokaryotes, usually leads to a low redox potential of the corresponding heme (3–6), and appears to be of special importance in sulfur-based energy metabolism. TsdA proteins catalyze the reversible formation of a sulfur-sulfur bond between the sulfane atoms of two thiosulfate molecules, yielding tetrathionate and releasing two electrons. TsdA enzymes of various source organisms exhibit different catalytic bias (7). Although the enzyme from the sulfur oxidizer *A. vinosum* is strongly adapted to catalyzing thiosulfate oxidation (2), TsdA from *Campylobacter jejuni* acts primarily as a tetrathionate reductase and enables the organism to use tetrathionate as an alternative electron acceptor for anaerobic respiration (8).

At present, it is largely unclear which redox carriers mediate the flow of electrons arising from thiosulfate oxidation into respiratory or photosynthetic electron chains. In several organ-

isms, including *Thiomonas intermedia, Sideroxydans lithotrophicus,* and *Pseudomonas stutzeri, tsdA* is immediately preceded by a gene encoding another diheme cytochrome, TsdB (1). TsdB itself is not reactive with thiosulfate but accepts electrons from TsdA even when TsdA and TsdB do not originate from the same organism (1). Kinetic data that quantitatively describe the interaction between TsdA and TsdB have not been published so far. In the anoxygenic phototrophic purple sulfur bacterium *Marichromatium purpuratum,* TsdA and TsdB form a fusion protein with TsdB constituting the N-terminal domain (7). TsdBA fusion proteins are also encoded in other members of the family Chromatiaceae, *i.e. Thiorhodococcus* sp. AK35 (D779_1816), *Thiocystis violascens* (Thivi_3993), *Thiorhodococcus drewsii* (ThidrDRAFT_3922), and *Thioflaviococcus mobilis* (Thimo_0460). However, TsdBA fusions are not a common trait in purple sulfur bacteria. In *A. vinosum,* a *tsdB* gene is not present (1).

In *A. vinosum,* the protein with the closest relationship to *T. intermedia* or *P. stutzeri* TsdB is Alvin_2879. This cytochrome c_4 (previously cytochrome $c_{553(550)}$) is membrane-bound (possibly via the hydrophobic protein Alvin_2880) and has a positive redox potential of $+330$ mV (9). Another candidate for accepting electrons from TsdA in purple anoxygenic phototrophic bacteria is the high potential iron-sulfur protein (HiPIP).[11] *A. vinosum* and *M. purpuratum* produce HiPIP, and as this protein has a quite positive reduction potential ($+350$ mV (10)) it would be well suited as an electron acceptor for TsdA. This proposal is corroborated by a previous report where a protein preparation with thiosulfate dehydrogenase activity from *A. vinosum* reduced HiPIP *in vitro* (11).

Here, we study Tsd(B)A enzymes from dedicated sulfur oxidizers and characterize in detail the interaction of TsdA with TsdB. Additionally, we pose the following question. Which proteins serve as immediate electron acceptors for either TsdA alone or the TsdBA fusion protein (when present)? It is furthermore intended to derive models for the electron flow involved.

Results

Characterization of TsdA and TsdB—UV-visible electronic absorbance spectroscopy, X-ray diffraction, and activity assays have revealed a number of characteristic features of *Av*TsdA (1, 2, 12). However, the electrochemical window in which the hemes are redox active remained unknown. To gain insight into this property, we mapped out the redox activity of *Av*TsdA adsorbed as an electroactive film on optically transparent mesoporous nanocrystalline SnO$_2$ electrodes. The spectrum of the enzyme-coated electrode equilibrated at $+302$ mV contained features typical of ferric *c*-type hemes superimposed on a small contribution from light scattering by the electrode material (Fig. 1). The Soret maximum at 406 nm and broad lower intensity features in the $\alpha\beta$-region are typical of those displayed by solutions of oxidized *Av*TsdA (1). When the electrode potential was lowered to -648 mV in 50-mV steps with a spectrum recorded after a 60-s pause at each desired potential (Fig.
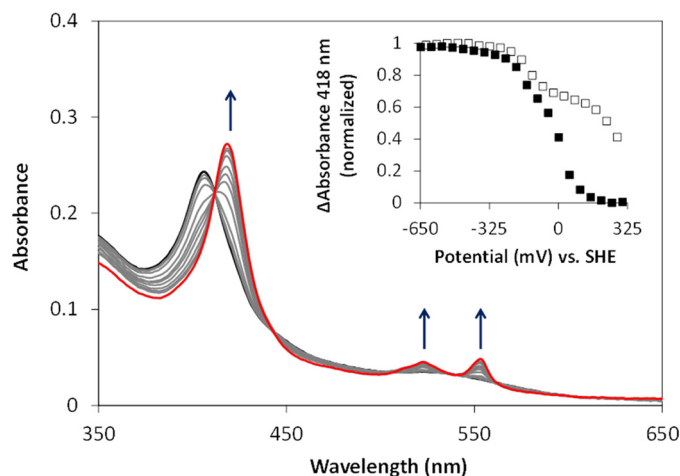

FIGURE 1. **Redox activity of *Av*TsdA adsorbed on a mesoporous nanocrystalline SnO$_2$ electrode.** Electronic absorbance was recorded with the electrode poised at $+302$ mV (*black*), $+152$ to -298 mV at 50-mV intervals (*gray*), and -648 mV (*red*). All potentials are quoted *versus* the standard hydrogen electrode (*SHE*). The *arrows* indicate increases in absorbance as the electrode potential was lowered. *Inset* shows the normalized change in absorbance at 418 nm against the applied potential as the enzyme was reduced (*closed squares*) and re-oxidized (*open squares*).

1), those features were replaced with peaks having maxima at 418, 523, and 553 nm, which are typical of dithionite-reduced enzyme (1). Variation of the Soret intensity at 418 nm with electrode potential revealed that the hemes were reduced between approximately $+150$ and -350 mV (Fig. 1, *inset, closed squares*).

The response of reduced *Av*TsdA to a stepwise increase of the electrode potential was assessed in a similar manner. The potential was raised in 50-mV steps, and the spectra were recorded after a 60-s pause at each potential (Fig. 1, *inset, open squares*). Between -648 and -98 mV, the variation in Soret intensity with the applied potential was very similar to that recorded on reduction. However, further increase of potential revealed significantly less oxidation than anticipated from the behavior seen on reduction of the enzyme. Importantly, spectra typical of the fully oxidized enzyme were measured after the electrode was poised at $+302$ mV for ~30 min. It was concluded that electrodic redox cycling of adsorbed *Av*TsdA was fully reversible but that full reduction occurred more quickly than complete re-oxidation. Further experiments confirmed that this behavior persisted over multiple rounds of reduction and re-oxidation. The spectral changes induced by variation of potential between -648 and -98 mV were rapidly reversed and accounted for ~35% of the change in absorbance at 418 nm when spectra of the fully oxidized and fully reduced forms of the enzyme were compared. By contrast, variations of electrode potential between -98 and $+302$ mV showed rapid reduction and much slower reoxidation, and the associated changes in absorbance accounted for ~65% of the total seen on full redox cycling of the enzyme. It was concluded that the slow reoxidation associated with higher potential redox event(s) was not a consequence of reversible redox events that occurred at lower potentials. Detailed inspection of the spectra provided no indication for the presence of high-spin ferric- or ferrous-heme.

The hysteretic nature of the plot of absorbance *versus* potential prevented Nernstian analysis to define the heme reduction

---

[11] The abbreviations used are: HiPIP, high potential iron-sulfur protein; PDB, Protein Data Bank; BisTris, 2-[bis(2-hydroxyethyl)amino]-2-(hydroxymethyl)propane-1,3-diol; r.m.s.d., root mean square deviation.
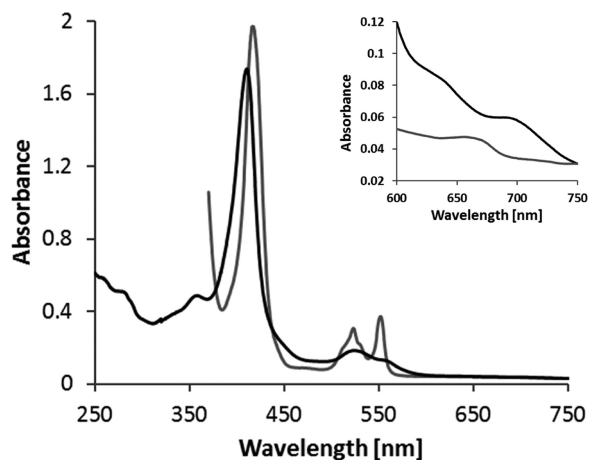
FIGURE 2. **UV-visible spectra of TsdB from *S. lithotrophicus.*** As the protein is partly reduced in the "as isolated" state, up to 170 μM ferricyanide were added to record the oxidized spectrum (*black line*). For full reduction of the protein, sodium dithionite was added (*gray line*). 100 mM Tris buffer, pH 8.0, with 150 mM NaCl and 2.5 mM desthiobiotin was used, and spectra are normalized to 750 nm. The oxidized spectrum exhibits a 700-nm peak indicating methionine as heme iron ligand. Protein concentration was 6 μM in the overview and 29 μM in the blowup.

potentials. Nevertheless, some further conclusions regarding the redox activity of *Av*TsdA can be proposed in light of the crystal structures reported (2, 12). The fully oxidized diheme cytochrome *Av*TsdA contains His/Cys coordination in heme 1 and His/Lys in heme 2. His/Cys-ligated hemes are typically distinguished from other low-spin *c*-type hemes by having much lower reduction potentials and smaller changes in extinction coefficient associated with the Fe(III)/(II) couple (4, 13). As a consequence, we propose that reduction of His/Cys-ligated heme 1 occurs reversibly between approximately −100 and −350 mV. Reduction of His/Lys-ligated heme 2 is proposed to occur between approximately +150 and −100 mV. *Av*TsdA X-ray structures reveal that this reduction is accompanied by a switch of Lys by Met as axial distal ligand to ferrous-heme 2 (2). Such a change of ligation would be expected to raise the reduction potential of heme 2. If the Met ligand is replaced slowly by Lys upon enzyme oxidation, this would account for the hysteretic nature of the redox behavior displayed by *Av*TsdA.

In contrast to TsdAs, TsdB proteins are not well characterized. The most closely related characterized cytochromes on a sequence level belong to the diheme cytochromes of the c_4 family (1). The recombinant TsdB protein from *T. intermedia* indeed binds two heme groups of 616.5 Da as the mass of 21,792.5 Da determined by MALDI-TOF mass spectrometry almost exactly matched the mass of 21,783.3 Da predicted for the mature recombinant protein, including Strep tag and two hemes. The same held true for recombinant *S. lithotrophicus* TsdB (measured mass, 22,864 Da, and predicted mass, 22,835 Da). UV-visible spectroscopy of pure recombinant TsdB from *S. lithotrophicus* is shown in Fig. 2. The spectrum conforms to that of *Ti*TsdB (1).

A sequence alignment of various TsdB proteins (Fig. 3) reveals two conserved methionine residues but no conserved histidines or cysteines indicating that both hemes of TsdB have axial coordination by His/Met. This is underpinned by the 700-nm peak in the spectrum, which is characteristic for methi-

onine as the sixth axial heme iron ligand (14) and corroborated by the *Mp*TsdBA crystal structure determined herein (see below). A shift of the Soret band from 411 to 417 nm upon reduction was observed. Moreover, there is a distinct δ band at 359 nm in the oxidized protein spectrum. In the reduced state, the α band was detected at 552 nm and the β band at 523 nm. A split α band characteristic for a number of c_4-type cytochromes, including those from purple sulfur bacteria, was not observed (9, 15). The UV-visible spectrum for oxidized TsdB exhibited a low intensity high spin feature at 620 nm similar to that noted for cytochrome c_4 from *P. stutzeri* (16). Obviously, the ferric form of TsdB holds a small fraction of high-spin heme probably caused by weakening of the Fe-S bond at one of the two hemes with concomitant partial dissociation of the methionine and formation of an Fe-aquo bond just as outlined for the *P. stutzeri* cytochrome (16).

The reduction potential of *Ti*TsdB was determined by potentiometry with a gold electrode (Fig. 4). The potential changes determined upon reduction and reoxidation of TsdB match well. The two hemes are redox active between −100 and +300 mV. Hysteresis was not observed, consistent with both hemes being His/Met-ligated. Ligand changes are not apparent.

TsdB Is an Electron-transferring Unit Tightly Interacting with TsdA—The interaction of TsdA and TsdB proteins was analyzed for the recombinant proteins from *S. lithotrophicus*. Upon analytical gel permeation chromatography *Sl*TsdA alone eluted at a volume corresponding to a molecular mass of 65 kDa, indicating dimerization of the protein under the conditions applied (monomer, 33,042 Da). In contrast, *Sl*TsdB behaved as a 22-kDa monomer (predicted molecular mass, 22,835 Da). When both proteins were produced simultaneously in *Escherichia coli* and purified employing the Strep tag attached to TsdA, a preparation was obtained that exhibited two heme stainable polypeptides. In size, these exactly matched *Sl*TsdB and *Sl*TsdA (Fig. 5). The co-purification of the two proteins is evidence for significant interaction between them. Upon size exclusion chromatography, *Sl*TsdA and *Sl*TsdB co-eluted again in fractions corresponding to a mass of 108 kDa, indicating formation of an $\alpha_2\beta_2$ heterodimer.

Characterization of the TsdBA Fusion Protein from M. purpuratum—The protein encoded by *tsdB-tsdA* gene fusion in *M. purpuratum* provides an exceptional possibility to study the complete tetraheme cytochrome for catalytic properties and internal electron transfer. A sequence alignment of *Mp*TsdBA with combined TsdB and TsdA sequences from *S. lithotrophicus* and *T. intermedia* shows significant similarity between the N-terminal region of *Mp*TsdBA and TsdB (amino acids 1–199 of *Mp*TsdBA and *Ti*TsdB share 45% sequence identity) and between the C-terminal region of *Mp*TsdBA and TsdA (amino acids 224–518 of *Mp*TsdBA compared with *Av*TsdA or *Ti*TsdA, 39 and 50% sequence identity, respectively). The heme distal ligands cysteine and methionine of TsdA as well as the two putative heme-ligating methionines are strictly conserved (Fig. 3). Therefore, we predicted *Mp*TsdBA to contain three His/Met ligated and one His/Cys ligated heme. UV-visible spectroscopy of *Mp*TsdBA protein is shown in Fig. 6. The presence of His/Met-ligated hemes in *Mp*TsdBA is substantiated by the 700-nm peak in the spectrum of the oxidized

```
MpTsdBA      PFERGRTLAEQGDAARGIVACAGCHRADGGGDEALGAARLAGLEPAYLATQIERFRAGQR      60
SlTsdB+TsdA  --ADEARNITLQGNKQGAPACQSCHGTDGGGTPSAGIPRLAGLNAAYIEQQLKNFRAGKR      58
TiTsdB+TsdA  -----------AAPPEAASCIACHGAGGMGNPAAGYPRLAGLPEQYLADQLRYFADGAR      48
                               *:  .** :  *  * :  *  *****  *:  *:.  *   *  *

MpTsdBA      SHPVMSPWAERLTPVDIAAVSAYYGALAPASN-ARAPSDVDAAAGRALAETGDWPERDLP     119
SlTsdB+TsdA  SNPIMQPIADLLTETEVTQVAAYYAALPVPLTTPQGADPALLRKGEAIATVGDWS-HEIP     117
TiTsdB+TsdA  NNAVMSGMAKPLSAAQVTALATYYSKLKPSGKPAPMTGAAAAEGERLALRGDWE-KGIP     107
                .. :*.  *. *: .:::  :::**. *   .        *. :*  ***    :  :*

MpTsdBA      ACVRCHGPGGVGAGAVFPPLAGQPYSYLLAQLQAWGTGRRHGEPMALMGAVAGRLDADEQ     179
SlTsdB+TsdA  ACFQCHGPNGKGIAPHFPAIAGQSALYISNQIEAWKSGTRSNDPAGIMKSVADKLSPEQI     177
TiTsdB+TsdA  ACIRCHGPGAVGVGENFPALVGQSAAYIEAQIKAWKDGSRSGDPLGIMHTVALRMTDAQT     167
             **.:**** . * . ** :.** *:  *::**  * * :* .** :** ::   :

MpTsdBA      RALAAYFATRPLAVADPADDLPDPSPPPATASVSTPAMTVAGANAVVPEHLGAVPAGRAE     239
SlTsdB+TsdA  EAVSAYLADQQSTNGNQK------------------------------ASETSTPTAA     205
TiTsdB+TsdA  QAVAQWLAAQPLSPTKSASAKH-------------------ADAPMAPPKSEINAAVG     206
             .*:: ::* :  :  .

MpTsdBA      AASRFTPPSRDALPEGPLGEMVRLGARLFRHTNTDPRSAPHVGNDQTCAGCHLDNGRRAD     299
SlTsdB+TsdA  KALVFTPPNDEEIPNNEFGKIVRQGKNIFEDTQH--YAKQYVGNSLNCVNCHLASGRKEN     263
TiTsdB+TsdA  TGAKFTPPPESAIPDDDFGKMVKLGRDIMLDTPK--YAKDYVGNTLSCVNCHTDAGRMAG     264
                .  ****  .:*:  :*::*:  *  :: .*     : .*** .*. ** **

MpTsdBA      ASPMWAAWVAYPAYRGKNQRVDTMAERIQQGCFRYSMNAQDSVSGQVPETNGLVLDALQSY     359
SlTsdB+TsdA  SSPLWAAYVRYPAYRAKNNKVNTYEERIQQGCFKYSLNGK------APAVDSPEMVALVTY     317
TiTsdB+TsdA  SAPLWAAYVSYPAYRGKNKKVNTFEERLQQGCFKFSQNGK------APPLGSKTLVALESY     318
              :*:***:* ***** .**:::*  **:**** .*.:    .*    : ** :*

MpTsdBA      IFWLATGAPTGDTAMSGRGYPRLQPPAEGFDRTRGAALYAEHCALCHGAEGEGLLVDGEV     419
SlTsdB+TsdA  SYWLATGAPVGA-KLKGAGYPEVPKPGLIPDANRGKTVFVENCQVCHGSNGEGKKVDGKY     376
TiTsdB+TsdA  SYWLSKGLPVDE-KVAGRGYPNLPEPQQAPDYVRGQKVYEAKCILCHAANGEGQYVNGET     377
              :**:.* *.   : * ***.:  *    *  **  ::  .* :**.::*** *:*:

MpTsdBA      VFPPLWGPRSYNWGAGMHRVDTAAAFIAANMPLLDTVRLTPQEAWDVAAYINAHERPQDP     479
SlTsdB+TsdA  IFPPLWGSESFNWGAGMHRINTAAAFIKANMPLSKGGTLTDQEAWDVATFVMSHERPQDP     436
TiTsdB+TsdA  VFPPLWGPKSFNWGAGMGSYKNAAKFIYANMPYGMSYSLSPQEAWDVAYFMDAQERPQDP     437
             :******* .*:****** ..** ** ****  *: ******* :: .::******

MpTsdBA      RFDGSVERTAARFHASPFDLYGEPLGVDGAVLGQGVAKD--                    518
SlTsdB+TsdA  RFKGNVAQTKKEYHDENC-RYGETV--NGKVLGGKHQTAAK                    474
TiTsdB+TsdA  RWQGSVAATRAKFHDSKFSLYGTKV--NGKLLGDIGAPKPR                    476
             *:.*.* * .:*.  .   **  ::  :*  :**
```

FIGURE 3. **Sequence alignment of *Mp*TsdBA and *Sl*TsdB + TsdA as well as *Ti*TsdB + TsdA.** Sequence comparison of TsdBA fusion protein of *M. purpuratum* (MARPU_02550) with the combined sequence of TsdB and TsdA from *S. lithotrophicus* (Slit_1877 and Slit_1878) and *T. intermedia* (Tint_1893 and Tint_2892). All signal peptide sequences were removed. Heme-binding motifs are indicated by *gray boxes*, and putative distal heme ligands are marked by *black edging*. Strictly conserved residues are marked with *asterisks*. TsdA sequences of *S. lithotrophicus* and *T. intermedia* start after the gap at amino acids 195 and 189, respectively.

FIGURE 4. **Determination of *Ti*TsdB reduction potential by potentiometry with a gold electrode.** Potentiometric determination of redox potentials of both TsdB hemes. Applied potential according to normalized values of the α-peak (553 nm) is shown. Reduction of TsdB (*black diamonds*) and re-oxidation of the protein (*gray squares*) was measured. 10 μM TsdB in phosphate buffer, pH 5.0, was used. *SHE*, standard hydrogen electrode.

FIGURE 5. **Analysis of purified *Sl*TsdA and *Sl*TsdB + A by SDS-PAGE.** 10–15 μg of *Sl*TsdA and *Sl*TsdB + A obtained after Strep tag affinity chromatography were loaded per lane on a 12.5% gel and stained for presence of heme. In case of *Sl*TsdB + A, both proteins were produced simultaneously in *E. coli* and purified on the basis of a Strep tag attached to TsdA.

protein. This absorption band is characteristic for methionine as heme iron ligand (14). A shift of the Soret band from 413 to 420 nm was observed upon reduction. Moreover, there is a distinct δ band at 363 nm in the oxidized protein spectrum. The α band is located at 553 nm, and the β band resides at 524 nm.

The partly reduced spectrum exhibits a low intensity high spin feature at 620 nm similar to *Av*TsdA (2). The $A_{413\ nm}/A_{280\ nm}$ for pure oxidized *Mp*TsdBA is 3.4.

Crystal Structure Determination and Model Quality of Mp TsdBA—To compare structural features of TsdA and TsdBA, to get a closer look into ligation of the four heme
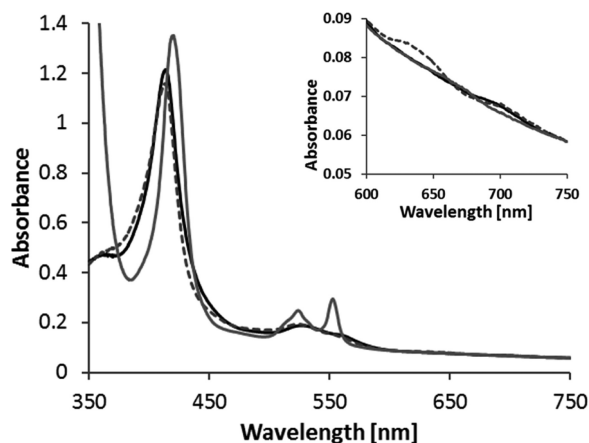
FIGURE 6. **UV-visible spectra of *Mp*TsdBA.** As the protein is slightly reduced in the "as isolated" state, 60 μM ferricyanide were added to record the oxidized spectrum (*black line*). For partial (*gray broken line*) and full reduction (*gray line*) of the protein, 0.33 and 5 mM sodium dithionite were added, respectively. 100 mM ammonium acetate buffer, pH 5, with 200 mM NaCl was used, and spectra are normalized to 750 nm. The oxidized spectrum exhibits a 700-nm peak indicating methionine as heme iron ligand and the partially reduced protein exhibits a feature at 630 nm. Protein concentration was 3.3 μM.

groups and to see how TsdA and TsdB domains are linked to each other, we have determined the X-ray structure of *Mp*TsdBA by Fe-SAD. Crystals belong to the hexagonal space group *H*32 with cell dimensions $a = b = 159.75$ Å and $c = 393.09$ Å. There are two molecules in the asymmetric unit corresponding to a Matthews coefficient (17) of 2.8 Å^3 Da^{-1} and a solvent content around 56%. The "as isolated" structure was refined to 2.75 Å resolution with R_{cryst} of 15.7% and R_{free} of 19.8% using a 141°-sweep of data with overall better statistics. Data collection and refinement statistics are depicted in Table 1. The high R_{meas} values observed for both sweeps are due, first, to the fine binning that autoPROC implements during data reduction, and second, to the fact that the crystal has some regions in the rotational space that are of bad quality. This is perfectly clear in the plots R_{meas} *versus* image number output by autoPROC (data not shown), highlighting that the high R_{meas} values are due to the crystal quality and not radiation damage. No evidence for radiation damage is also observed in a $m|F_o| - m|F_o|$ map calculated using both data sweeps (data not shown). *Mp*TsdBA is numbered without taking into account its 23-amino acid signal peptide that is removed upon transport into the periplasm. The model comprises the following residues of the mature recombinant protein: Pro^1–Leu^{191} and Arg^{237}–Val^{515} (chain A) and Pro^1–Ala^{192} and Ala^{240}–Ala^{516} (chain B), eight heme molecules, two thiosulfate ions, two chloride ions, seven ethylene glycols, two 1,2-propanediols and one triethylene glycol, and 113 water molecules. Electron density maps are of good quality except for the C-terminal His tag and the disordered loop connecting TsdB and TsdA domains. This region (45 amino acid residues long in chain A and 47 in chain B) has a predicted loop-like secondary structure and is not included in the final model, because no electron density was observed. Moreover, some parts of the map are somewhat "noisy" with positive and negative difference map peaks in the solvent region that could not be modeled.

Overall Fold and Similar Structures of MpTsdBA—*Mp*TsdBA is organized into two domains, an N-terminal TsdB domain and a C-terminal TsdA domain (Fig. 7*A*). Each domain includes two subdomains that are related by a pseudo-2-fold symmetry axis. Each subdomain consists of four α-helices surrounding a heme group, the typical class I *c*-type cytochrome topology. This has been previously reported for the *Av*TsdA crystal structure (2, 12) and is also observed for the *M. purpuratum* N-terminal TsdB domain. The four subdomains superimpose with r.m.s.d. of 1.3–3.0 Å for ~70 aligned Cα atoms corresponding to sequence similarities between 10 and 38%.

The final model coordinates were submitted to the DALI server (18), showing no similar structures to the complete *Mp*TsdBA arrangement. However, several hits structurally match each domain of the enzyme separately. The highest matches to *Mp*TsdB domain were cytochrome c_4 from *P. stutzeri* (PDB code 1M6Z), cytochrome c_{552} from *Acidithiobacillus ferroxidans* (PDB code 1H1O), the cytochrome subunit of flavocytochrome *c* sulfide dehydrogenase from *A. vinosum* (PDB code 1FCD), and flavocytochrome *c* from *Thermochromatium tepidum* (PDB code 3VRD), with *Z*-scores of 22.7 to 17.5, r.m.s.d. of 2.0–2.4 Å, and sequence identities between 30 and 23%.

The highest hit for the *Mp*TsdA domain was *Av*TsdA (4V2K and 4WQ9) with a *Z*-score of 30.6 (with 20% sequence identity and r.m.s.d. of 1.4 and 1.2 Å, respectively), followed by SoxAX from *Rhodovulum sulfidophilum* (2OZ1), the SoxD subunit of SoxCD from *Paracoccus pantotrophus* (2XTS), and the SoxA subunits of SoxAX from *Starkeya novella* (3OA8) and *P. pantotrophus* (2C1D). *Z*-scores ranged from 12–7.4 and r.m.s.d.s from 2.1 to 4.7 Å.

Heme Coordination in the "As Isolated" MpTsdBA—The *Mp*TsdBA crystal structure shows four heme groups per chain packed as a wire with closest iron-to-iron distances between 15 and 19 Å and shortest edge-to-edge distances of 3.5 to 6.6 Å (Fig. 7, *B* and *C*). This agrees well with other multiheme cytochrome structures that show edge-to-edge distances of 4–8 Å (19, 20).

The four hemes are covalently bound to the polypeptide chain through thioether bonds formed by cysteine residues Cys^{21} and Cys^{24} for heme 1, Cys^{121} and Cys^{124} for heme 2, Cys^{287}and Cys^{290} for heme 3, and Cys^{402} and Cys^{405} for heme 4 (Fig. 8, *A–D*). Moreover, the structure confirmed the spectroscopic evidence gathered showing that this tetraheme cytochrome *c* has three hemes (hemes 1, 2, and 4) with His/Met coordination (Fig. 8, *A*, *B*, and *D*). Axial ligation by histidine and cysteine is typical for the active site of TsdA proteins (2, 12). Indeed, heme 3 exhibits axial ligation by His^{291}, and the Sγ atom of Cys^{330} is located in close vicinity to the heme iron such that it could serve as the sixth ligand. However, the 2.9 Å distance between the sulfur and the iron atom precludes direct ligation (Fig. 8, *C*, *E*, and *F*). It has been shown earlier that the Sγ atom of the corresponding active site cysteine (Cys^{96}) in TsdA from *A. vinosum* can adopt two different conformations by rotation of the cysteine Cα–Cβ bond. Therefore, the sulfur atom switches between iron-ligating and iron-non-ligating states (2). The non-ligating conformation has been proposed as

TABLE 1
Data reduction and refinement statistics for *Mp*TsdBA structure

	142.65°-sweep data set (refinement)	Full 360° data set (Fe-SAD phasing)
PDB code	5LO9	
Data collection		
Synchrotron	ESRF (Grenoble, France)	
Beamline	ID-29	
Wavelength (Å)	1.7236	
Space group	*H*32	
Unit cell		
a, b, c (Å)	159.75, 159.75, 393.09	159.89, 159.89, 392.99
α, β, γ (o)	90.0, 90.0, 120.0	
Resolution range[a] (Å)	113.13–2.75 (2.76–2.75)	130.99–2.82 (2.83–2.82)
Total no. of reflections	377,526 (2187)	891,650 (6064)
No. of unique reflections	50,199 (461)	49,983 (442)
Completeness (%)	99.0 (87.8)	99.6 (94.2)
Anomalous completeness (%)	98.7 (84.8)	99.6 (94.1)
Multiplicity	7.5 (4.7)	19.0 (13.7)
Anomalous multiplicity	3.9 (2.5)	9.9 (7.0)
$\langle I/\sigma(I)\rangle$	14.9 (2.0)	15.4 (2.4)
R_{meas}[b] (%)	11.7 (70.6)	25.5 (184.7)
R_{pim} (%)	5.7 (41.8)	8.1 (69.2)
$CC_{1/2}$[c] (%)	99.7 (63.8)	99.4 (75.7)
Refinement		
R_{cryst}[d] (%)	15.7 (25.9)	
R_{free}[e] (%)	19.8 (30.0)	
No. of non-H atoms		
Protein	7028	
Ligands	330	
Waters	113	
r.m.s.d. bonds (Å)	0.013	
r.m.s.d. angles (°)	1.50	
Protein residues	Pro[1]–Leu[191] and Arg[237]–Val[515] (chain A), Pro[1]–Ala[192] and Ala[240]–Ala[516] (chain B)	
Ramachandran plot		
Most favored (%)	97.6	
Allowed (%)	2.4	
Outliers (%)	0	
Rotamer outliers (%)	0.9	
Clashscore	2.69	
MolProbity score[f]	1.28	
B-Factors (Å²)		
Protein	52.04	
Ligands/ions	50.43	
Waters	45.06	

[a] Information in parentheses refers to the last resolution shell.
[b] $R_{meas} = \Sigma_h\Sigma_l|I_{hl} - \langle I_h\rangle|/\Sigma_h\Sigma_l \langle I_h\rangle$, where I_{hl} is the Ith observation of reflection h and $\langle I_h\rangle$.
[c] $CC_{1/2}$ is as described previously (57).
[d] $R_{cryst} = \Sigma_h|F_{obs(h)}| - |F_{calc(h)}|/\Sigma_h|F_{obs(h)}|$, where $F_{obs(h)} - F_{calc(h)}$ are the observed and calculated structure factors for reflection h, respectively.
[e] R_{free} was calculated as R_{factor} but using only 5% of reflections randomly selected and omitted from refinement.
[f] MolProbity score provides a single number that represents the central MolProbity protein quality statistics; it is a log-weighted combination of clashscore, Ramachandran not favored and bad side-chain rotamers, giving one number that reflects the crystallographic resolution at which those values would be expected.

an essential intermediate step in the catalytic cycle, possibly involving covalent attachment of a substrate molecule (2, 12).

Remarkably, in the "as isolated" structure of *Mp*TsdBA a thiosulfate ion is indeed covalently bound to Cys[330]. A *polder* map supporting the modeling of the thiosulfate ion is depicted in Fig. 8*E*. The thiosulfate is oriented such that the S1-S2 plane points toward the heme plane, and the S2 atom lies 2.06 Å away from the Sγ atom of Cys[330], thus being within covalent bond distance. Thiosulfate was refined to 66% occupancy in chain A and 72% in chain B. The Sγ of Cys[330] (full occupancy) superposes well with the Sγ atom of Cys[96] in *Av*TsdA with bisulfite (PDB code 4WQB). Here, the Sδ of persulfurated Cys[96] superimposes with S2 of thiosulfate in the *Mp*TsdBA structure. In both structures, these ligand-bound cysteines are not coordinating the heme. Noteworthy, some continuity in the electron density maps is still seen on heme 3, even though Cys[330] is not ligated to the heme iron. We expect *Mp*TsdBA Cys[330] to coordinate the heme when no ligand/substrate is present, similar to what is observed in *Av*TsdA crystal structures (2, 12).

The thiosulfate substrate lies in a cleft accessible from the solvent to Cys[330] and heme 3. This cavity is delineated by the side chains of positively charged residues Arg[314], Lys[316], Arg[326], Arg[438], and Arg[480] (Fig. 8*F*), which have been previously proposed to be involved in the orientation and stabilization of the substrate for catalysis (2, 12). Some positive electron density ($m|F_o| - D|F_c|$) is present near the substrate, although no density is observed in $2m|F_o| - D|F_c|$ maps (even at low contours). This electron density is observed between the Nζ atom of Lys[316] and the plane formed by the three oxygen atoms of the thiosulfate ion (although independent from the density observed for the thiosulfate ion itself). Because this electron density was not amenable to refinement, nothing was included in the final 3D structure. Furthermore, heme 3 seems to display another residual conformation with one of the propionates alternating between this cavity and a cleft above the heme plane delineated by Arg[377], Arg[381], and the N main chain atoms of Gly[378] and Tyr[379]. This motion is illustrated by the different conformation modeled for heme 3 in both chains, either pointing toward the
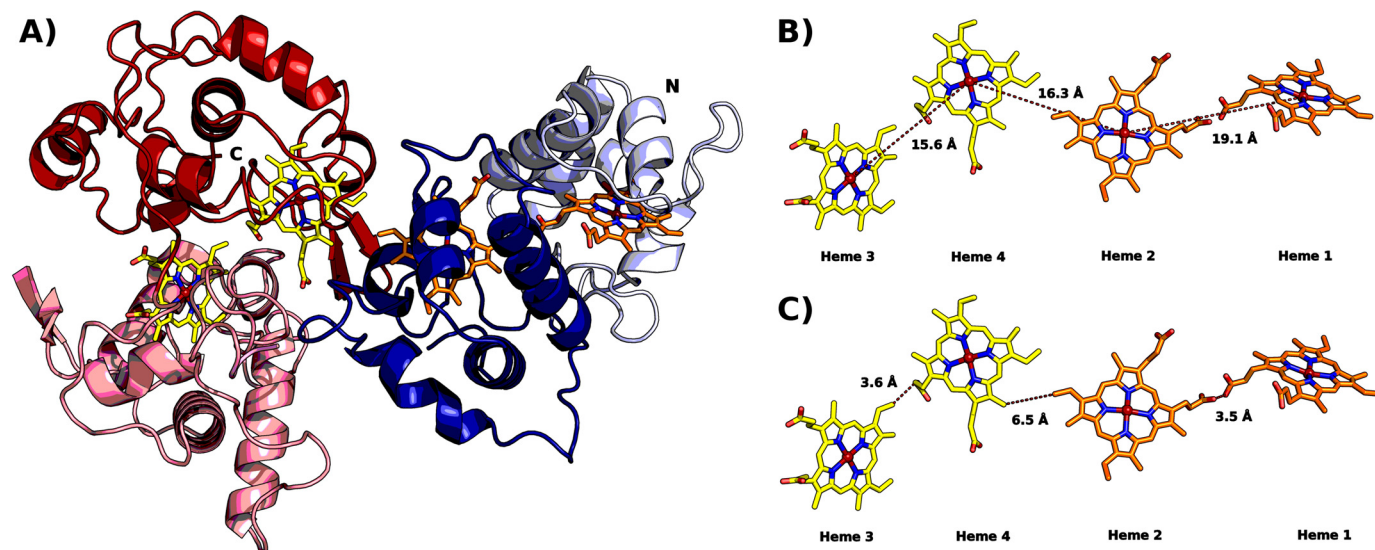
FIGURE 7. **X-ray structure of *Mp*TsdBA and heme arrangement.** *A,* overall fold with TsdB N-terminal domain (residues 1–193) depicted in *blue* and TsdA C-terminal domain (residues 240–516) in *red*; the two shades in each domain represent the respective sub-domains (1–90 and 91–193 for TsdB and 240–377 and 378–516 for TsdA). The heme prosthetic groups are colored by atom type (*orange* or *yellow* for carbon, *blue* for nitrogen, *red* for oxygen, and *dark red* for iron). *B,* Fe-to-Fe distances; *C,* closest edge-to-edge distances.

active site cavity, in chain A (Fig. 8*E*), or toward the cleft above the heme plane, in chain B (Fig. 8, *C* and *F*). However, this possible alternate conformation could not be properly refined, and therefore it was not added to the crystallographic model.

Reactivity with External Electron Acceptors—To test different electron acceptors for TsdA and TsdBA, we performed enzyme activity assays with TsdB from *T. intermedia, A. vinosum* cytochrome c_4 (Alvin_2879), and *A. vinosum* HiPIP as electron acceptors. All three potential electron acceptors were produced as recombinant proteins in *E. coli.*

Previously, it had been shown that TsdB from *T. intermedia* is not reactive with thiosulfate but that it is instantaneously reduced when TsdA is added in the presence of thiosulfate (1). Here, we succeeded in obtaining quantitative kinetic data for a homologous system by analyzing electron transfer between TsdA and TsdB from *S. lithotrophicus.* Just as *Ti*TsdB, *Sl*TsdB alone is not reduced by addition of thiosulfate. An enzyme activity assay with *Sl*TsdA as the catalyst and *Sl*TsdB as the electron acceptor resulted in a specific activity of 6.3 units mg^{-1} for *Sl*TsdA. $S_{0.5}$ for thiosulfate was determined to be 0.04 mM. This unambiguously identified *Sl*TsdB as an effective electron acceptor for TsdA from the same organism. However, a heterologous approach yielded a different result; with 0.6 units mg^{-1} the specific activity of *Av*TsdA with TsdB from *T. intermedia* amounted to only one-tenth that determined for the homologous system, whereas $S_{0.5}$ for thiosulfate (0.03 mM) resided in a similar range.

In a further series of experiments, *Av*TsdA activity was tested with Cyt c_4 originating from the same host. It should be noted that the recombinant cytochrome was electrophoretically pure and that it exhibited exactly the same spectral features as Cyt c_4 purified from *A. vinosum* cells, including the characteristic split α-band (9). The specific activity of *Av*TsdA with *Av*Cyt c_4 as the electron acceptor amounted to 0.6 units mg^{-1} and was thus not found to be higher than with TsdB from a different source orga-

nism. Therefore, we exclude those diheme cytochromes as efficient electron acceptors for *Av*TsdA *in vitro* as well as *in vivo.*

HiPIP from *A. vinosum*, a protein with a positive reduction potential (+350 mV (10)), was tested as another potential candidate for accepting electrons from *Av*TsdA as well as from *Mp*TsdBA. Indeed, both thiosulfate dehydrogenases reacted efficiently with *A. vinosum* HiPIP (Fig. 9 and Table 2). *Av*TsdA exhibited a higher V_{max} with HiPIP as electron acceptor, whereas *Mp*TsdA featured an especially low $S_{0.5}$ value for thiosulfate when the reaction was measured with HiPIP as electron acceptor. In both cases, $S_{0.5}$ for thiosulfate was much lower with HiPIP than with ferricyanide as the electron acceptor indicating cooperativity between the electron-transferring heme 2 and the active site heme 1. *A. vinosum* and *M. purpuratum* both encode HiPIP in their genome, and both thiosulfate dehydrogenases exhibit substantial specific activity with HiPIP as electron acceptor *in vitro*, leading us to conclude that HiPIP also serves as an efficient *in vivo* electron acceptor for Tsd(B)A in both organisms.

Discussion

In our approach to find suitable electron acceptors for TsdA-type thiosulfate dehydrogenases, we first focused on TsdB, a diheme cytochrome encoded upstream of TsdA in a number of different organisms. As demonstrated here for the proteins from *S. lithotrophicus* and earlier for those from *T. intermedia* (1), TsdA and TsdB enzymes interact strongly with each other and form an $\alpha_2\beta_2$ heterodimer. The same arrangement has been described for thiosulfate dehydrogenase from *Halothiobacillus neapolitanus* (21), which consists of heme c binding subunits of 27 and 33 kDa conforming in size with TsdA and TsdB, respectively.

In this work, a redox range of −300 to +150 mV was determined for *Av*TsdA, whereas *Ti*TsdB is redox active between −100 and +300 mV. Generalizing this finding, we state that the
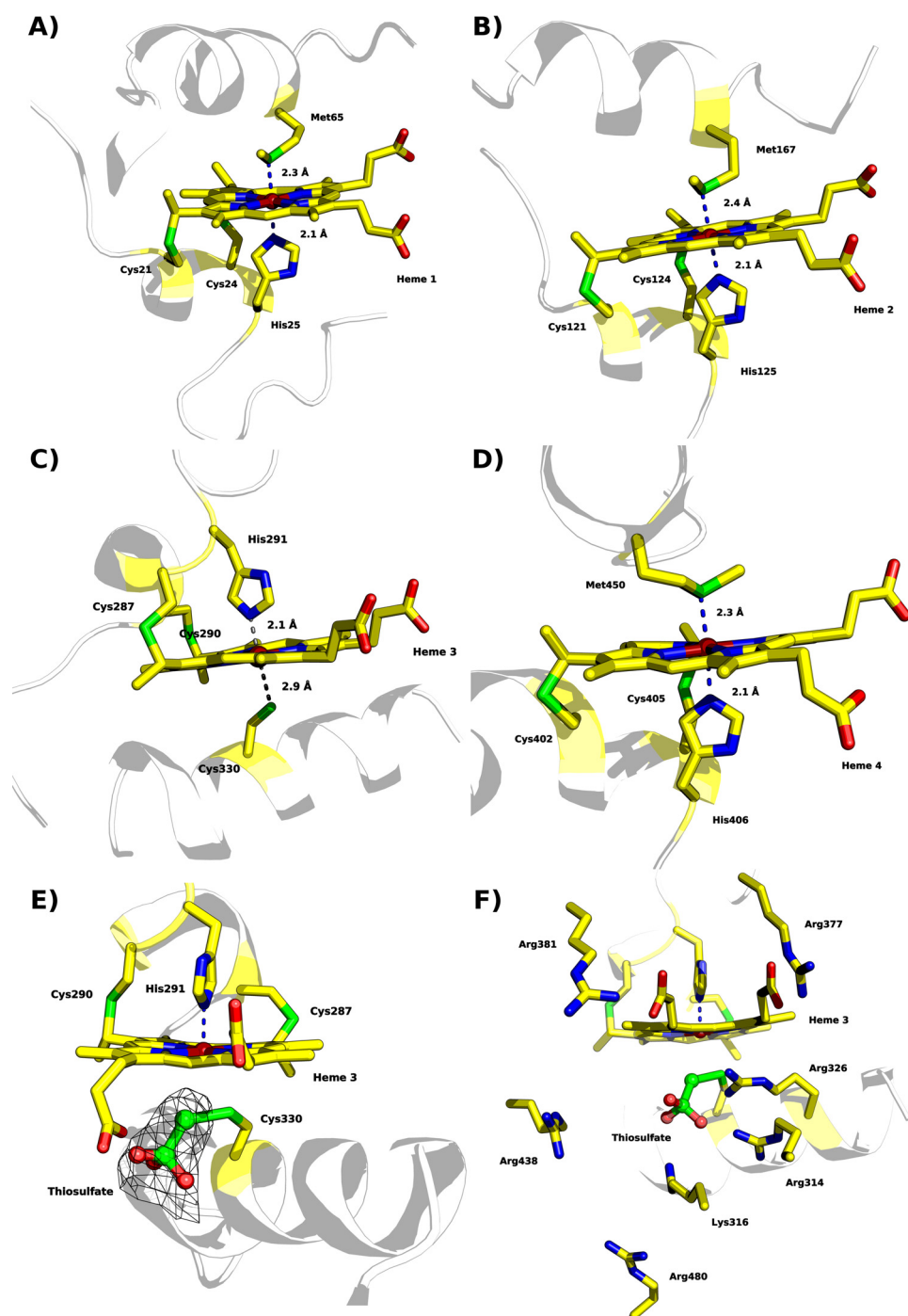
FIGURE 8. **Heme coordination of "as isolated" *Mp*TsdBA (PDB code 5LO9).** *A,* heme 1 is coordinated by His[25] and Met[65]. *B,* heme 2 is coordinated by His[125] and Met[167]. *C,* heme 3 is ligated to His[291] but not to Cys[330]. The distance of Sγ to the heme iron is 2.9 Å and thus not close enough for direct ligation. Thiosulfate covalently bound to Sγ of Cys[330] is not shown here for clarity. Presence of thiosulfate is illustrated in detail in *E* and *F*. *D,* Heme 4 is ligated by His[406] and Met[450]. *E,* heme 3 with Sγ of Cys[330] covalently bound to thiosulfate, displayed in *ball and stick*, and *polder* map electron density contoured at 6σ level depicted as a *black mesh*. *F,* heme 3 in a similar view as in *E* but with positively charged residues surrounding the substrate cleft depicted as *sticks*. Scheme representation is shown in *pale gray* with heme moieties and coordinating amino acid residues shown as *sticks*; color code as in Fig. 7 with sulfur atoms in *green*.

overall reduction potential of TsdB is more positive than that of TsdA, which should enable electron flow from TsdA to TsdB. Indeed, reduction of *Ti*TsdB by *Av*TsdA had been shown previously (1) and was verified here for the proteins from *S. lithotrophicus*. Enzyme activity assays further revealed *Sl*TsdB as an effective electron acceptor for *Sl*TsdA but not for *Av*TsdA. This was not surprising as *A. vinosum* does not contain a gene encoding TsdB (Table 3).

In *A. vinosum*, the gene with strongest similarity to *tsdB* is Alvin_2879. The encoded high potential diheme cytochrome c_4 has been suggested to play a role in transferring electrons to the photosynthetic reaction center (9). The *M. purpuratum* genome also encodes a protein (Marpu_15750) with high similarity to *A. vinosum* Cyt c_4 (78% identity on the sequence basis; see Table 3). In the anoxygenic phototroph *Rubrivivax gelatinosus*, a related cytochrome c_4 indeed has an established func-

tion as an alternative electron donor to the photosynthetic reaction center (22). It was therefore feasible to assume that electrons generated by thiosulfate oxidation could be shuttled to the reaction center via cytochrome c_4 in purple sulfur bacteria. However, the very low specific activity of AvTsdA with *A. vinosum* cytochrome c_4 essentially precludes such a role (Fig. 10).

In many anoxygenic photosynthetic bacteria, the periplasmic high potential iron-sulfur protein is well known to shuttle electrons between the cytochrome bc_1 complex and the photosynthetic reaction center during cyclic electron flow (23–26). This function has also been firmly established for the protein from *A. vinosum* (24, 27). Here, we demonstrate that HiPIP is a suitable electron acceptor for Tsd(B)A from *A. vinosum* and *M. purpuratum in vitro*, identifying this protein as the most likely electron carrier between the thiosulfate-oxidizing enzyme and the reaction center during growth in the light. It should be noted that a direct interaction between Tsd(B)A and
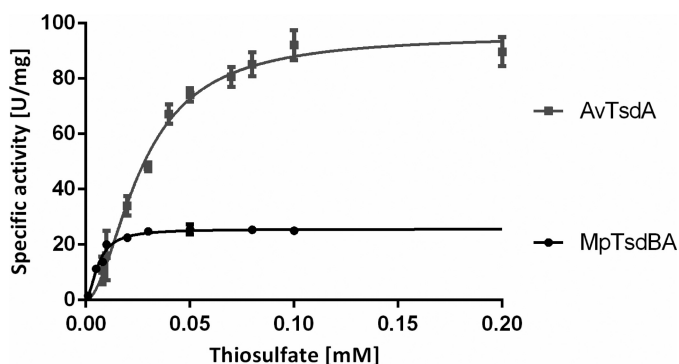
FIGURE 9. **Thiosulfate oxidation catalyzed by *Av*TsdA and *Mp*TsdBA with HiPIP as electron acceptor.** Enzyme assays with *Av*TsdA were performed in 100 mM ammonium acetate buffer, pH 5, at 30 °C with 8 nM enzyme. Activity measurements with *Mp*TsdBA were performed in 100 mM ammonium acetate buffer, pH 5.2, with 200 mM NaCl at 25 °C and with 3.9 nM enzyme. In both assays 10 μM HiPIP and 40 μM ferricyanide were used. A change in absorbance was measured at 480 nm. *v versus* [S] plots were fitted to the Hill equation.

TABLE 2

Thiosulfate oxidation of *Av*TsdA and *Mp*TsdBA with ferricyanide and HiPIP

Enzyme assays with *Av*TsdA were performed in 100 mM ammonium acetate buffer, pH 4, at 30 °C with 8 nM enzyme. Activity measurements with *Mp*TsdBA were performed in 100 mM ammonium acetate buffer, pH 5.2, with 200 mM NaCl at 25 °C and with 3.9 nM enzyme. In assays with HiPIP as electron acceptor, 10 μM HiPIP and 40 μM ferricyanide were used, and absorbance at 480 nm was followed. In activity assays with ferricyanide as electron acceptor, 1 mM ferricyanide was used, and the absorbance at 420 nm was measured. The units for V_{max} are μmol min^{-1} mg protein^{-1}. *v versus* [S] plots were fitted to the Hill equation.

Electron acceptor	Enzyme	V_{max}	$S_{0.5}$	k_{cat}	$_{cat}/S_{0.5}$
		units mg^{-1}	*μM*	*s^{-1}*	*mM^{-1} s^{-1}*
Ferricyanide	*Av*TsdA	31,419 ± 2408	835 ± 119	14,091	16,875
	*Mp*TsdBA	3011 ± 108	179 ± 21	2794	15,611
HiPIP	*Av*TsdA	96 ± 3	27 ± 2	43	1595
	*Mp*TsdBA	26 ± 1	6 ± 0	24	4000

the photosynthetic reaction center cannot be completely excluded so far.

Many purple sulfur bacteria, including *A. vinosum,* are capable of chemolithotrophic growth on reduced sulfur compounds and oxygen under microaerobic conditions (28). Accordingly, cbb_3 as well as ubiquinol oxidases are encoded in their genomes. Although the standard reduction potential of the thiosulfate/tetrathionate couple (+198 mV (7)) appears too positive to feed electrons directly into the quinone pool, and from there to oxygen, delivery of electrons originating from the thiosulfate to tetrathionate conversion to cbb_3 oxidase is certainly feasible. In fact, HiPIP has been reported to be involved in bacterial respiratory chains (29, 30) and is a prime candidate for electron transport between Tsd(B)A and the terminal oxidase in those organisms where it is present. However, in chemotrophs like *T. intermedia* or *S. lithotrophicus*, the situation must be different because these bacteria do not contain HiPIP. In fact, for these organisms, it is not exactly established so far which periplasmic proteins deliver electrons to cbb_3 oxidase, regardless of the electron donor oxidized. For *S. lithotrophicus* it is assumed that the *c*-type cytochrome MtoD (Slit_2498) can transfer electrons stemming from iron oxidation to cbb_3 oxidase and the cytochrome bc_1 complex (31). In the *T. intermedia* genome, there are two *c*-type cytochromes (Tint_2575 and Tint_3060) with 36 and 42% sequence identity to *S. lithotrophicus* MtoD, respectively, which may serve a similar function. It may be possible that thiosulfate dehydrogenase delivers electrons to the MtoD(-like) cytochrome, which then shuffles the electrons to the terminal oxidase.

Nevertheless, an alternative scenario is also possible when we consider the similarity between TsdB and cytochromes of the c_4-type (about 49% sequence identity between *Ti*TsdB and Cyt c_4 from *Achromobacter xylosoxidans* or *Pseudomonas protegens*). Cytochromes of the c_4-type have been reported to donate electrons to cbb_3-type cytochrome *c* oxidases in various oxygen-respiring bacteria (32–34), and we therefore consider the possibility that TsdB serves as a direct electron donor to cbb_3 oxidase at least in tetrathionate-forming thiosulfate oxidizers that neither contain HiPIP nor any cytochrome c_4 homolog except TsdB.

We have determined the first three-dimensional structure of *M. purpuratum* TsdBA, where TsdA is fused with its electron acceptor TsdB. It showed heme arrangement with characteristic class I *c*-type cytochrome topology, unveiling their relative heme spatial disposition and providing insights into the electron flow during enzymatic reaction. In the *Mp*TsdBA structure, a thiosulfate ion is covalently bound to Sγ of Cys^{330} in heme 3, although the protein was produced in and purified from *E. coli* without the addition of thiosulfate to media or buffers. This implies high affinity of the enzyme to thiosulfate, which is possibly present in the complex growth medium in
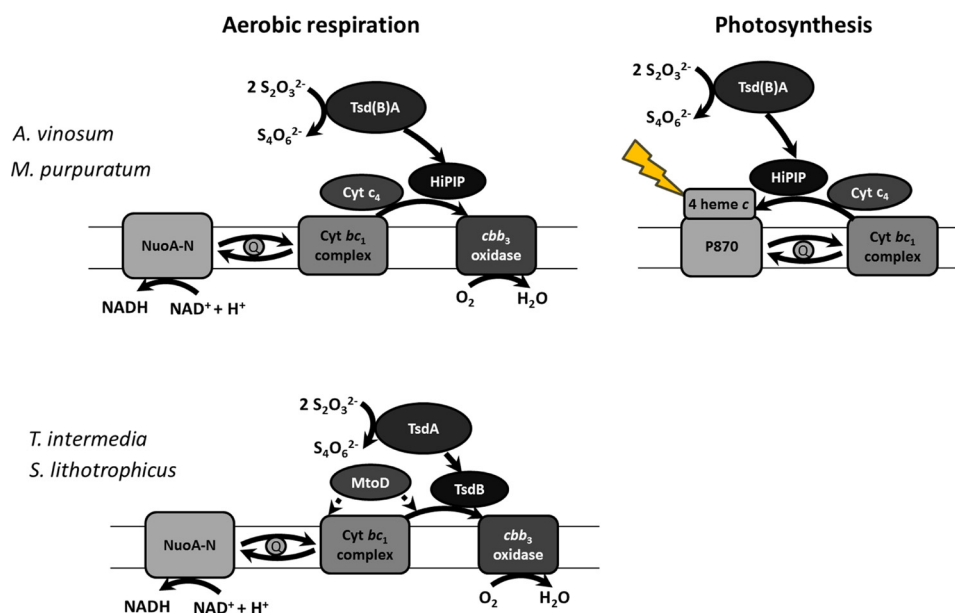
TABLE 3

Occurrence of genes encoding TsdA and putative electron acceptors in the genome sequenced organisms relevant to this study

Organism	TsdA	TsdB	Cyt c_4	HiPIP
A.vinosum DSM 180^T	Alvin_0091		Alvin_2879	Alvin_2274
M. purpuratum 984 (DSM 1591^T)	Marpu_02550 (TsdBA fusion)	Marpu_15750	Marpu_11560	
S. lithotrophicus ES-1 (ATCC 700298^T)	Slit_1878	Slit_1877		
T. intermedia K12 (DSM 18155^T)	Tint_2892	Tint_2893		

Aerobic respiration

Photosynthesis

FIGURE 10. **Role of periplasmic electron transfer proteins in aerobic respiration or photosynthesis of *A. vinosum*, *M. purpuratum*, *S. lithotrophicus*, and *T. intermedia*.** All organisms contain genes for NuoA-N (Alvin_2418–2430 + Alvin_2412, Marpu_04365–04430, Slit_1070–1083, and Tint_2255–2268), the cytochrome bc_1 complex (Alvin_0068–0070, Marpu_01465–01475, Slit_0130–0132, and Tint_2192–2194), and cbb_3 oxidase (Alvin_0781–0784, Marpu_02795–02810, Slit_0411–0414, and Tint_1070–1073). Moreover, *A. vinosum* and *M. purpuratum* can gain energy by photosynthetic growth. HiPIP can transfer electrons to the photosynthetic reaction center (23, 24) as well as to cbb_3 oxidase (29, 30). Cytochrome c_4 also is known to transfer electrons to the photosynthetic reaction center (22) as well as to cbb_3 oxidase (32–34) in some bacteria. For *S. lithotrophicus*, it is assumed that MtoD (Slit_2498) can transfer electrons to cbb_3 oxidase and the cytochrome bc_1 complex (31).

very low concentrations. It should be noted that recombinant *Av*TsdA and also several SoxA proteins have been isolated with the active site cysteine in a partially or fully persulfurated state (2, 35–37). This has been interpreted as indication for temporary binding of thiosulfate and subsequent incomplete catalysis. Just as proposed here, thiosulfate was assumed to originate from the *E. coli* growth medium (2).

Regardless of its source, the covalent attachment of a complete thiosulfate molecule to the *Mp*TsdBA active site cysteine strongly supports the hypothesis that tetrathionate formation from two thiosulfate molecules proceeds via a rhodanese-like reaction mechanism involving a thiosulfate transfer reaction with a thiosulfate molecule covalently bound to the active site cysteine as an essential intermediate in the catalytic cycle (2, 12). This type of mechanism has been illustrated in detail by Grabarczyk *et al.* (12) for TsdA from *A. vinosum*. A rhodanese-like reaction cycle has also repeatedly been depicted and discussed for the closely related SoxXA protein, but it could not be unambiguously proven before (4, 35). The *Mp*TsdBA structure provides conclusive evidence that the reactions catalyzed by TsdA as well as SoxXA enzymes indeed involve a cysteine *S*-thiosulfonate intermediate that is formed once the first thiosulfate molecule is positioned in the substrate binding pocket by positively charged amino acid side chains (Arg[314], Lys[316], Arg[326], and Arg[438] in *Mp*TsdBA, Fig. 8*F*). The latter also stabilized the cysteine *S*-thiosulfonate group once it had formed. Formation of the cysteine *S*-thiosulfonate releases two electrons that reduce the iron atoms of the two hemes in TsdA to the Fe(II) state. Heme reoxidation by an external electron acceptor is then likely to be followed by a thiol-disulfide exchange reaction that proceeds via an attack of the sulfane

atom of a second thiosulfate molecule on the thiosulfonate group (12).

We conclude that catalysis of thiosulfate oxidation by Tsd(B)A enzymes and very probably also that by SoxXA proteins involves formation of a covalent adduct between the sulfane sulfur atom of thiosulfate and the Sγ of the active site cysteine. When present, TsdB is the immediate electron acceptor of TsdA. TsdB is very likely able to transfer electrons directly to the cbb_3 terminal oxidase. In organisms containing HiPIP, this electron carrier is likely to act as an additional shuttle not only between Tsd(B)A and the terminal oxidase during oxygen respiration but also between Tsd(B)A and the photosynthetic reaction center during photolithotrophic growth in the light.

Experimental Procedures

Bacterial Strains, Plasmids, and Growth Conditions—Table 4 lists the bacterial strains and plasmids used for this study. *E. coli* BL21 (DE3) was used for recombinant protein production and was grown in LB medium. *E. coli* DH5α was used for molecular cloning.

Recombinant DNA Techniques—All general molecular genetics techniques were described earlier (38). Restriction enzymes, T4 ligase, and *Pfu* DNA polymerase were obtained from Thermo Scientific (Schwerte, Germany) and used according to the manufacturer's instructions. Oligonucleotides for cloning were obtained from Eurofins MWG (Ebersberg, Germany).

Construction of Expression Plasmids—*A. vinosum tsdA* and *T. intermedia tsdB* genes coding for the mature proteins without the signal peptides were amplified and cloned as described

TABLE 4
E. coli strains and plasmids used in this study

Strains and plasmids	Description	Ref. or source
Strains		
E. coli DH5α	F⁻ φ80d *lacZ*ΔM15 Δ(*lacZYA-argF*)U169 *recA1 endA1hsdR17* (rk⁻ mk⁺) *supE44* λ⁻ *thi-1 gyrA relA1*	56
E. coli BL21 (DE3)	F⁻ *ompT hsd*S$_B$ (r$_B$⁻m$_B$⁻) *gal dcm met*(DE3)	Novagen
Plasmids		
pEC86	Cm^r, product from pEC66 and pACYC184 with *E. coli ccmABCDEFGH* genes	40
pET-22b (+)	Ap^r, T7 promoter, lac operator, C-terminal His tag, pelB leader	Novagen
pASK-IBA3 plus	Ap^r, *tetA* promoter/operator, C-terminal Strep tag	IBA (Göttingen)
pET_ MarpuDRAFT_1194	Ap^r, *tsdA* from *M. purpuratum* (Marpu_02550) was cloned into pET-22b (+) with NdeI and XhoI, C-terminal His tag	7
pASK-IBA*Tint_tsdB*	Ap^r, *tsdB* from *T. intermedia* cloned into pASK-IBA3 plus with BsaI, C-terminal Strep tag	1
pASK-IBA3plus-*slit1877*	Ap^r; *tsdB* from *S. lithotrophicus* (Slit_1877) cloned into pASK-IBA3 plus with BsaI, C-terminal Strep tag	This study
pASK-IBA3plus-*slit1878*	Ap^r; *tsdA* from *S. lithotrophicus* (Slit_1878) cloned into pASK-IBA3 plus with BsaI, C-terminal Strep tag	This study
pASK-IBA3plus-*slit1877-slit1878*	Ap^r; *tsdBA* from *S. lithotrophica* (Slit_1877-Slit_1878) cloned into pASK-IBA3 plus with BsaI, C-terminal Strep tag	This study
pET-soxXAK-Strep	Ap^r, *soxXAK*, including fragment cloned into pET-22b(+) together with C-terminal Strep tag by use of XbaI and HindIII	This study
pET-Alvin2274-C-Strep	Ap^r, *hip* gene coding for HiPIP from *A. vinosum* (Alvin_2274) cloned into pET-soxXAK-Strep with NdeI and NcoI, C-terminal Strep tag	This study
pPR-IBAAvtsdA	Ap^r; *tsdA* from *A. vinosum* (Alvin_0091) cloned into pASK-IBA3, C-terminal Strep tag	1
pASK-IBA3plus_Alvin_2879	Ap^r; Alvin_2879 from *A. vinosum* cloned into pASK-IBA3 plus with BsaI, C-terminal Strep tag	This study

earlier (1). The *tsdA* gene (Slit_1878), the *tsdB* gene (Slit_1877), and the *tsdBA* gene combination (Slit_1877-Slit1878) from *S. lithotrophicus* ES-1 (ATCC 700298^T) were amplified from genomic DNA with primers Slit1877_fw/Slit1877_rev, Slit1878_fw/Slit1878_rev, and Slit1877_fw/Slit1878_rev (Table 5), respectively. The native signal peptides encoding sequences were included in all three cases. The *tsdBA* gene fusion (Marpu_02550) from *M. purpuratum* 984 (DSM 1591^T) was amplified without its original signal peptide encoding sequence using primers MarpuDR1194_for/MarpuDR1194_rev. The gene Alvin_2879, encoding a cytochrome c_4 with similarity to TsdB, was amplified with primers 2879+Sp-for and 2879-rev such that the signal peptide-encoding sequence was included. The HiPIP-encoding *hip* (Alvin_2274) gene (39) was amplified without the signal peptide-encoding sequence applying primers Alvin2274-C-strep_for/Alvin2274-C-strep_rev. Chromosomal DNA from *A. vinosum* DSM 180^T served as the template. For cloning of *SltsdB*, *SltsdA*, *SltsdB-tsdA*, and Alvin_2879, primers included BsaI restriction sites, and the digested PCR products were cloned into BsaI-digested pASK-IBA3plus (IBA, Göttingen) resulting in vectors pASK-IBA3plus-slit1877, pASK-IBA3plus-slit1878, pASK-IBA3plus-slit1877-slit1878, and pASK-IBA3plus_Alvin_2879. For the cloning of *MptsdBA* into pET-22b(+) (Novagen), the restriction enzymes NdeI and XhoI were used yielding plasmid pET_MarpuDRAFT_1194. Plasmid pET-Alvin2274 was constructed by cloning *Avhip* into a modified pET-22b(+) vector (pET-soxXAK-strep) encoding a C-terminal Strep tag. This vector had previously been constructed in the course of cloning the *A. vinosum soxXAK* genes. PCR primers with NdeI (XAK-NdeI-for) and NcoI (XAK-NcoI-rev) sites were used, and the resulting fragment was cloned into pET-22b(+). The XbaI/NcoI fragment of the resulting plasmid was cloned into pASK-IBA3. XbaI and HindIII served for excising the *soxXAK* genes together with the Strep tag-encoding sequence. The XbaI/HindIII fragment was cloned between the XbaI and HindIII sites of pET22b(+) giving pET-soxXAK-strep. Replacing the *soxXAK* genes in this construct by *Avhip* yielded *A. vinosum* HiPIP fused to a C-terminal Strep tag.

Overproduction, Purification, and Preparation of Recombinant Proteins—*Av*TsdA and *Ti*TsdB were produced as described before (1). For production of *S. lithotrophicus* TsdA, *Sl*TsdB and the simultaneous production of *Sl*TsdB and *Sl*TdsA *E. coli* BL21(DE3) cells containing pASK-IBA3plus-slit1877, pASK-IBA3plus-slit1878, or pASK-IBA3plus-slit1877-slit1878 and pEC86 (40) were cultured in 700 ml of LB media supplemented with 100 µg ml⁻¹ ampicillin and 25 µg ml⁻¹ chloramphenicol at 37 °C and 180 rpm after inoculation with an overnight pre-inoculum in a (1:50) dilution. At an OD$_{600 nm}$ of 0.4 to 0.6, 200 ng ml⁻¹ anhydrotetracycline were added, and the appropriate culture was switched to 25 °C and 90 rpm in case of TsdB production. Cells were harvested after 18 h. *Mp*TsdBA and HiPIP were produced in *E. coli* BL21(DE3) cells containing pET_MarpuDRAFT_1194 or pET-Alvin2274 and pEC86 (40). After 2 or 0.5% inoculation with a pre-culture, the cells were grown in 700 ml of LB medium containing 100 µg ml⁻¹ ampicillin and 25 µg ml⁻¹ chloramphenicol at 37 °C and 180 rpm. At an OD$_{600 nm}$ of 0.5 to 0.6, the cultures were switched to 25 °C and 120 rpm for about 18 h. For production of *Av*Cyt c_4 (Alvin_2879), *E. coli* BL21(DE3) cells containing pASK-IBA3plus_Alvin_2879 and pEC86 (40) were cultured in 400 ml of LB medium, 100 µg ml⁻¹ ampicillin, and 25 µg ml⁻¹ chloramphenicol at 37 °C and 180 rpm after 2% inoculation with a preculture. At OD$_{600 nm}$ ~0.5, 200 ng ml⁻¹ anhydrotetracycline were added, and the culture was switched to 25 °C and 90 rpm for 18 h. Harvested cells were resuspended in 100 mM Tris-HCl buffer, pH 8.0, containing 150 mM NaCl and lysed by sonication. After removal of insoluble cell material by centrifugation (10,000 × g for 25 min at 4 °C), *Sl*TsdA, *Sl*TsdB, *Sl*TsdB + TsdA, *A. vinosum* cytochrome c_4 (Alvin_2879), and *Av*TsdA were purified by Strep-Tactin (IBA, Göttingen, Germany) affinity chromatography according to the manufacturer's instructions. *Mp*TsdBA was purified by nickel-chelate (Qiagen, Hilden, Germany) affinity chromatography according to the manufacturer's instructions and then subjected to a size-exclusion chromatography step performed on a HiLoad 16/60 Superdex 75-pg column (GE Healthcare) using an ÄKTApuri-

TABLE 5
Primers used in this study

Primer	Sequence 5′–3′	Ref.
MarpuDR1194_for	CGGAGGGATCCTCATATGACGCATCTC	7
MarpuDR1194_rev	GACCTGCTCGAGATCCTTGGC	7
Slit1877_fw	ATGGTAGGTCTCAAATGAAGCAAATATTACTAGCAGCATTAAC	This study
Slit1877_rev	ATGGTAGGTCTCAGCGCTTTTCTGGTTTCCATTGGTTGATTGT	This study
Slit1878_fw	ATGGTAGGTCTCAAATGAAGAATCCCATCGCTATCGCCAT	This study
Slit1878_rev	ATGGTAGGTCTCAGCGCTCTTTGCTGCAGTCTGGTGCTTTC	This study
XAK-NdeI-for	GGAGATTTCATATGCCGTTGAACGTCTCACACCG	This study
XAK-NcoI-rev	ATGGCTCCATGGTATCGAGACCGATCGAGC	This study
Alvin2274-C-strep_for	GCCCATATGTCCGCTCCCGCCAAT	This study
Alvin2274-C-strep_rev	CAACGGCCCATGGCCCGGCCTTCAG	This study
2879+Sp-for	ATGGTAGGTCTCAAATGAAGAAGACTTGGCTGACAACGGT	This study
2879-rev	ATGGTAGGTCTCAGCGCTCTTCGACAGGCCCTGGATGTAC	This study

fier system (GE Healthcare). The column was equilibrated with 20 mM Tris-HCl buffer, pH 7.5, and 150 mM NaCl. TsdB and TsdA from *S. lithotrophicus* were analyzed by the same procedure either separately or as a mixture of both proteins. In this case, the Superdex 75 column was equilibrated with 100 mM Tris-HCl buffer, pH 7.5, and 150 mM NaCl. The column was calibrated with the molecular weight marker kit MW-GF-70 (GE Healthcare). All purified proteins were desalted with 5 ml of HiTrap Desalting columns (GE Healthcare) and concentrated with Amicon Ultra-15 centrifugal filter units (Merck Millipore). Recombinant *S. lithotrophicus* proteins were stored in 100 mM sodium acetate buffer pH 5 at −70 °C, *A. vinosum* Cyt c_4 in 20 mM Tris-HCl buffer, pH 7.5, at 4 °C, *Mp*TsdBA in 20 mM Tris-HCl buffer, pH 7.5, with 150 mM NaCl at −70 °C, and HiPIP in 20 mM Tris-HCl, pH 7, at 4 °C. The concentration of purified proteins was determined with the BCA kit from Pierce. For assessment of purity, SDS-PAGE was performed, and the proteins were visualized either by Coomassie or heme staining techniques.

UV-visible Spectroscopy with TsdA in Solution—UV-visible spectra were recorded between 250 and 750 nm with an Analytik Jena Specord 210 (Analytik Jena, Jena, Germany).

Assay of Thiosulfate Oxidase Activity with Ferricyanide—Thiosulfate-dependent ferricyanide reduction was measured by following the decrease in absorbance at 420 nm ($\epsilon = 1.09$ mM^{-1} cm^{-1}). Enzyme activity measurements with *Av*TsdA at pH 4 are described in Ref. 2. Activity measurements with *Mp*TsdBA were performed with 1 mM ferricyanide at 25 °C in 100 mM ammonium acetate buffer, pH 5.2, with 200 mM NaCl. Assays were started by addition of TsdA, and data were recorded in a Specord 210 spectrophotometer (Analytik Jena, Jena, Germany). Activity is expressed as micromoles of tetrathionate produced per min and milligram of protein on the basis of one tetrathionate formed per two ferricyanides reduced. In the case of enzymes that use two molecules of the same substrate (here thiosulfate) primary *v* versus [S] plots provide the best way to examine the data (41). Data were fitted to the empirical Hill equation (Equation 1) using GraphPad Prism (version 6; GraphPad).

$$v = \frac{V_{\text{max}}[S]^n}{K + [S]^n} \qquad \text{(Eq. 1)}$$

The Hill equation resembles the classical Henri-Michaelis-Menten equation; however, the *n* term allows accounting for non-hyperbolic shapes. A substrate concentration $[S]_{0.5}$ can be

reported that yields half-maximal velocity and is characteristic of the process. The constant *K*, which is not equivalent to K_m, characterizes enzyme-substrate interaction. The relationship between *K* and $[S]_{0.5}$ is $K = [S]_{0.5}{}^n$.

Assay of Thiosulfate Oxidase Activity with HiPIP—For assays of electron transfer from thiosulfate to the electron acceptor HiPIP, 10 μM HiPIP preoxidized with 40 μM ferricyanide were used. The reaction was started by addition of enzyme and followed by the absorbance decrease at 480 nm. A molar extinction coefficient at 480 nm of 10.7 mM^{-1} cm^{-1} (10) was used. Measurements with *Av*TsdA were performed in 100 mM ammonium acetate buffer, pH 5, at 30 °C and with *Mp*TsdBA in 100 mM ammonium acetate buffer, pH 5.2, with 200 mM NaCl at 25 °C.

Assay of Thiosulfate Oxidase Activity with TsdB or AvCyt c_4—Thiosulfate-dependent reduction of *T. intermedia* TsdB or *A. vinosum* Cyt c_4 was measured by following the increase in absorbance at 417 nm ($\epsilon_{\Delta417\,\text{nm}} = 99$ mM^{-1} cm^{-1}) for *Ti*TsdB or *Sl*TsdB and at 420 nm ($\epsilon_{\Delta420\,\text{nm}} = 55$ mM^{-1} cm^{-1} (9)) for *Av*Cyt c_4. The extinction coefficient for TsdB was calculated with the help of the Beer-Lambert law using distinct concentrations of *Ti*TsdB and the differences in absorbance at 417 nm in the reduced and oxidized spectra. A value averaged from measurements with three different protein concentrations was derived. Assays of *Sl*TsdA activity with *Sl*TsdB as electron acceptor were carried out in 100 mM ammonium acetate buffer, pH 4, at 25 °C. *Av*TsdA activity with *Ti*TsdB was assayed in 100 mM ammonium acetate buffer, pH 5, at 30 °C, whereas *Av*TsdA activity with *Av*Cyt c$_4$ was determined in 100 mM ammonium acetate buffer, pH 5.5, at 25 °C.

Determination of Redox Properties of AvTsdA Adsorbed on a Mesoporous Nanocrystalline SnO$_2$ Electrode—An optically transparent mesoporous nanocrystalline SnO$_2$ electrode coated with *Av*TsdA was prepared using the previously described method (42) with adsorption from a solution of 10 μM *Av*TsdA, 2 mM neomycin, 50 mM NaCl, 50 mM HEPES, pH 7. The enzyme-coated electrode was rinsed with 2 mM neomycin, 50 mM NaCl, 50 mM HEPES, pH 7, to remove unbound protein, taken into a N$_2$-filled chamber (atmospheric O$_2$ < 2 ppm) and immersed in an anaerobic solution of the same composition within a previously described spectroelectrochemical cell (42). The cell was sealed, removed from the anaerobic chamber, and inserted into a Jasco V650 UV-visible spectrophotometer thermostated at 4 °C and flushed with argon to maintain anaerobic status. Spectral contributions from light

scattering by the electrode were minimized by placing a bare SnO_2 electrode (*i.e.* having no adsorbed enzyme) in the reference beam of the spectrophotometer. The electronic absorbance of the as prepared enzyme-coated electrode revealed features indicative of a mixture of ferric and ferrous hemes. After the electrode had been poised at +302 mV for 45 min, the spectrum revealed that the enzyme had been converted to the fully oxidized all ferric state. To determine the redox activity of *Av*TsdA, the electrode potential was swept from +302 to −648 mV at a scan rate of 5 mV s^{-1} with a pause of 150 s every 50 mV. At 60 s into each pause, a spectrum was measured before the scan continued. Reoxidation of the sample was performed in a similar manner. Spectra are presented after equating absolute absorbance at 600 nm to account for potential dependent changes in the spectral contributions that arise from scattering by the electrode material.

Redox Potentiometry with TsdB in Solution Measured with a Gold Electrode—The reduction potential of *Ti*TsdB was measured with help of a gold-platinum electrode system under anoxic conditions. The electrode extended into a cuvette containing the protein solution (20 μM) and redox mediators (*N,N*-dimethyl-1,4-phenylenediamine, *p*-benzoquinone, trimethylhydroquinone, phenazine, 1,4-naphthoquinone, and 1,2-naphthoquinone at 2 μM each) in 20 mM MOPS buffer, pH 6, and was connected to a potentiometer. *Ti*TsdB was reduced by changing the applied potential from −150 to 450 mV. Subsequential decrease of the potential again to −150 mV led to reoxidation of the protein. A spectrum was recorded every 2 min and potentials converted to values *versus* standard hydrogen electrode.

Crystallization, Data Collection, Structure Determination, and Refinement—*Mp*TsdBA at a concentration of 3.2 mg ml^{-1} in 20 mM BisTris-HCl, pH 6.5, and 150 mM NaCl was crystallized in 10% (w/v) PEG 8000, 0.1 M Tris-HCl, pH 7.0, 0.2 M MgCl$_2$, and 10 mM trimethylamine hydrochloride (as additive) by vapor-diffusion hanging-drop method at 20 °C. Crystallization droplets contained 1.0 μl of protein, 0.8 μl of precipitant, and 0.2 μl of additive and were equilibrated against a 200-μl reservoir solution (26% (w/v) PEG 3350). Crystals were cryoprotected with No. 2 solution of CryoProtX screen (Molecular Dimensions), consisting of 25% (v/v) diethylene glycol, 25% (v/v) 1,2-propanediol, and 25% (v/v) glycerol. X-ray diffraction data were collected at a wavelength of 1.7236 Å on beamline ID-29 of the European Synchrotron Radiation Facility (ESRF, Grenoble, France). Data were indexed and integrated with XDS (43), and the space group was determined with POINTLESS (44) and scaled with AIMLESS (45, 46), all within the autoPROC (47) data processing pipeline. An R_{free} flag was created at this stage corresponding to 5% of the measured reflections of the data set. The structure was determined by single wavelength anomalous dispersion method around the iron edge (Fe-SAD), employing a high multiplicity data collection strategy using the autoSHARP module (48), within the SHARP package (49). Iterative model building and refinement cycles were performed with COOT (50) and BUSTER-TNT (51) (at early stages of refinement), followed by phenix.refine (52), until a complete model was built and refinement convergence achieved. Friedel mates were kept separately and refinement

was carried out against I(+)/SIGI(+),I(−)/SIGI(−). A *polder* map (an omit map that excludes the bulk solvent around the omitted region) and $m|F_o| - m|F_o|$ map were calculated within the PHENIX package of programs. The Ramachandran diagram was assessed with RAMPAGE (53), and the model was validated with MolProbity (54) as implemented in PHENIX. All figures were rendered with PyMOL, Schrödinger LLC (55).

References

1. Denkmann, K., Grein, F., Zigann, R., Siemen, A., Bergmann, J., van Helmont, S., Nicolai, A., Pereira, I. A., and Dahl, C. (2012) Thiosulfate dehydrogenase: a widespread unusual acidophilic *c*-type cytochrome. *Environ. Microbiol.* **14,** 2673–2688
2. Brito, J. A., Denkmann, K., Pereira, I. A., Archer, M., and Dahl, C. (2015) Thiosulfate dehydrogenase (TsdA) from *Allochromatium vinosum*: structural and functional insights into thiosulfate oxidation. *J. Biol. Chem.* **290,** 9222–9238
3. Pires, R. H., Venceslau, S. S., Morais, F., Teixeira, M., Xavier, A. V., and Pereira, I. A. (2006) Characterization of the *Desulfovibrio desulfuricans* ATCC 27774 DsrMKJOP complex–a membrane-bound redox complex involved in the sulfate respiratory pathway. *Biochemistry* **45,** 249–262
4. Bradley, J. M., Marritt, S. J., Kihlken, M. A., Haynes, K., Hemmings, A. M., Berks, B. C., Cheesman, M. R., and Butt, J. N. (2012) Redox and chemical activities of the hemes in the sulfur oxidation pathway enzyme SoxAX. *J. Biol. Chem.* **287,** 40350–40359
5. Reijerse, E. J., Sommerhalter, M., Hellwig, P., Quentmeier, A., Rother, D., Laurich, C., Bothe, E., Lubitz, W., and Friedrich, C. G. (2007) The unusual redox centers of SoxXA, a novel *c*-type heme-enzyme essential for chemotrophic sulfur-oxidation of *Paracoccus pantotrophus*. *Biochemistry* **46,** 7804–7810
6. Kappler, U., Bernhardt, P. V., Kilmartin, J., Riley, M. J., Teschner, J., McKenzie, K. J., and Hanson, G. R. (2008) SoxAX cytochromes, a new type

of heme copper protein involved in bacterial energy generation from sulfur compounds. *J. Biol. Chem.* **283,** 22206–22214

7. Kurth, J. M., Dahl, C., and Butt, J. N. (2015) Catalytic protein film electrochemistry provides a direct measure of the tetrathionate/thiosulfate reduction potential. *J. Am. Chem. Soc.* **137,** 13232–13235

8. Liu, Y.-W., Denkmann, K., Kosciow, K., Dahl, C., and Kelly, D. J. (2013) Tetrathionate stimulated growth of *Campylobacter jejuni* identifies TsdA as a new type of bi-functional tetrathionate reductase that is widely distributed in bacteria. *Mol. Microbiol.* **88,** 173–188

9. Cusanovich, M. A., and Bartsch, R. G. (1969) A high potential cytochrome *c* from *Chromatium vinosum* chromatophores. *Biochim. Biophys. Acta* **189,** 245–255

10. Bartsch, R. G. (1978) Purification of $(4Fe-4S)^{1-2-}$ ferredoxins (high-potential iron-sulfur proteins) from bacteria. *Methods Enzymol.* **53,** 329–340

11. Fukumori, Y., and Yamanaka, T. (1979) A high-potential nonheme iron protein (HiPIP)-linked, thiosulfate-oxidizing enzyme derived from *Chromatium vinosum*. *Curr. Microbiol.* **3,** 117–120

12. Grabarczyk, D. B., Chappell, P. E., Eisel, B., Johnson, S., Lea, S. M., and Berks, B. C. (2015) Mechanism of thiosulfate oxidation in the SoxA family of cysteine-ligated cytochromes. *J. Biol. Chem.* **290,** 9209–9221

13. Du, J., Sono, M., and Dawson, J. H. (2011) The H93G myoglobin cavity mutant as a versatile scaffold for modeling heme iron coordination structures in protein active sites and their characterization with magnetic circular dichroism spectroscopy. *Coord. Chem. Rev.* **255,** 700–716

14. Miles, C. S., Manson, F. D., Reid, G. A., and Chapman, S. K. (1993) Substitution of a haem-iron axial ligand in flavocytochrome b_2. *Biochim. Biophys. Acta* **1202,** 82–86

15. Branca, R. M., Bodó, G., Várkonyi, Z., Debreczeny, M., Osz, J., and Bagyinka, C. (2007) Oxygen and temperature-dependent structural and redox changes in a novel cytochrome c_4 from the purple sulfur bacterium *Thiocapsa roseopersicina*. *Arch. Biochem. Biophys.* **467,** 174–184

16. Nissum, M., Karlsson, J.-J., Ulstrup, J., Jensen, P. W., and Smulevich, G. (1997) Resonance Raman characterization of the di-heme protein cytochrome c_4 from *Pseudomonas stutzeri*. *J. Biol. Inorg. Chem.* **2,** 302–307

17. Matthews, B. W. (1968) Solvent content of protein crystals. *J. Mol. Biol.* **33,** 491–497

18. Holm, L., and Rosenström, P. (2010) Dali server: conservation mapping in 3D. *Nucleic Acids Res.* **38,** W545–W549

19. Igarashi, N., Moriyama, H., Fujiwara, T., Fukumori, Y., and Tanaka, N. (1997) The 2.8 Å structure of hydroxylamine oxidoreductase from a nitrifying chemoautotrophic bacterium, *Nitrosomonas europaea*. *Nat. Struct. Biol.* **4,** 276–284

20. Taylor, P., Pealing, S. L., Reid, G. A., Chapman, S. K., and Walkinshaw, M. D. (1999) Structural and mechanistic mapping of a unique fumarate reductase. *Nat. Struct. Biol.* **6,** 1108–1112

21. Visser, J. M., de Jong, G. A., Robertson, L. A., and Kuenen, J. G. (1996) Purification and characterization of a periplasmic thiosulfate dehydrogenase from the obligately autotrophic *Thiobacillus* sp. W5. *Arch. Microbiol.* **166,** 372–378

22. Ohmine, M., Matsuura, K., Shimada, K., Alric, J., Verméglio, A., and Nagashima, K. V. (2009) Cytochrome c_4 can be involved in the photosynthetic electron transfer system in the purple bacterium *Rubrivivax gelatinosus*. *Biochemistry* **48,** 9132–9139

23. Bartsch, R. G. (1991) The distribution of soluble metallo-redox proteins in purple phototrophic bacteria. *Biochim. Biophys. Acta* **1058,** 28–30

24. Kennel, S. J., Bartsch, R. G., and Kamen, M. D. (1972) Observations on light-induced oxidation reactions in the electron transport system of *Chromatium*. *Biophys. J.* **12,** 882–896

25. Nagashima, K. V., Matsuura, K., Shimada, K., and Verméglio, A. (2002) High-potential iron-sulfur protein (HiPIP) is the major electron donor to the reaction center complex in photosynthetically growing cells of the purple bacterium *Rubrivivax gelatinosus*. *Biochemistry* **41,** 14028–14032

26. Lieutaud, C., Nitschke, W., Verméglio, A., Parot, P., and Schoepp-Cothenet, B. (2003) HiPIP in *Rubrivivax gelatinosus* is firmly associated to the membrane in a conformation efficient for electron transfer towards the photosynthetic reaction centre. *Biochim. Biophys. Acta* **1557,** 83–90

27. Verméglio, A., Li, J., Schoepp-Cothenet, B., Pratt, N., and Knaff, D. B. (2002) The role of high-potential iron protein and cytochrome c_8 as alternative electron donors to the reaction center of *Chromatium vinosum*. *Biochemistry* **41,** 8868–8875

28. Kämpf, C., and Pfennig, N. (1980) Capacity of Chromatiaceae for chemotrophic growth. Specific respiration rates of *Thiocystis violacea* and *Chromatium vinosum*. *Arch. Microbiol.* **127,** 125–135

29. Hochkoeppler, A., Jenney, F. E., Jr., Lang, S. E., Zannoni, D., and Daldal, F. (1995) Membrane-associated cytochrome c_γ of *Rhodobacter capsulatus* is an electron carrier from the cytochrome bc_1 complex to the cytochrome c oxidase during respiration. *J. Bacteriol.* **177,** 608–613

30. Bonora, P., Principi, I. I., Monti, B., Ciurli, S., Zannoni, D., and Hochkoeppler, A. (1999) On the role of high-potential iron-sulfur proteins and cytochromes in the respiratory chain of two facultative phototrophs. *Biochim. Biophys. Acta* **1410,** 51–60

31. Beckwith, C. R., Edwards, M. J., Lawes, M., Shi, L., Butt, J. N., Richardson, D. J., and Clarke, T. A. (2015) Characterization of MtoD from *Sideroxydans lithotrophicus*: a cytochrome *c* electron shuttle used in lithoautotrophic growth. *Front. Microbiol.* **6,** 332

32. Arai, H., Kawakami, T., Osamura, T., Hirai, T., Sakai, Y., and Ishii, M. (2014) Enzymatic characterization and in vivo function of five terminal oxidases in *Pseudomonas aeruginosa*. *J. Bacteriol.* **196,** 4206–4215

33. Barco, R. A., Emerson, D., Sylvan, J. B., Orcutt, B. N., Jacobson Meyers, M. E., Ramírez, G. A., Zhong, J. D., and Edwards, K. J. (2015) New insight into microbial iron oxidation as revealed by the proteomic profile of an obligate iron-oxidizing chemolithoautotroph. *Appl. Environ. Microbiol.* **81,** 5927–5937

34. Chang, H. Y., Ahn, Y., Pace, L. A., Lin, M. T., Lin, Y. H., and Gennis, R. B. (2010) The diheme cytochrome c_4 from *Vibrio cholerae* is a natural electron donor to the respiratory cbb_3 oxygen reductase. *Biochemistry* **49,** 7494–7503

35. Bamford, V. A., Bruno, S., Rasmussen, T., Appia-Ayme, C., Cheesman, M. R., Berks, B. C., and Hemmings, A. M. (2002) Structural basis for the oxidation of thiosulfate by a sulfur cycle enzyme. *EMBO J.* **21,** 5599–5610

36. Dambe, T., Quentmeier, A., Rother, D., Friedrich, C., and Scheidig, A. J. (2005) Structure of the cytochrome complex SoxXA of *Paracoccus pantotrophus*, a heme enzyme initiating chemotrophic sulfur oxidation. *J. Struct. Biol.* **152,** 229–234

37. Kilmartin, J. R., Maher, M. J., Krusong, K., Noble, C. J., Hanson, G. R., Bernhardt, P. V., Riley, M. J., and Kappler, U. (2011) Insights into structure and function of the active site of SoxAX cytochromes. *J. Biol. Chem.* **286,** 24872–24881

38. Dahl, C., Schulte, A., Stockdreher, Y., Hong, C., Grimm, F., Sander, J., Kim, R., Kim, S.-H., and Shin, D. H. (2008) Structural and molecular genetic insight into a wide-spread bacterial sulfur oxidation pathway. *J. Mol. Biol.* **384,** 1287–1300

39. Brüser, T., Trüper, H. G., and Dahl, C. (1997) Cloning and sequencing of the gene encoding the high potential iron-sulfur protein (HiPIP) from the purple sulfur bacterium *Chromatium vinosum*. *Biochim. Biophys. Acta* **1352,** 18–22

40. Arslan, E., Schulz, H., Zufferey, R., Künzler, P., and Thöny-Meyer, L. (1998) Overproduction of *Bradyrhizobium japonicum* c-type cytochrome subunits of the cbb_3 oxidase in *Escherichia coli*. *Biochem. Biophys. Res. Commun.* **251,** 744–747

41. Segel, I. H. (1993) *Enzyme Kinetics: Behaviour and Analysis of Rapid Equilibrium and Steady-state Enzyme Systems*, Wiley-Interscience, New York

42. Marritt, S. J., Kemp, G. L., Xiaoe, L., Durrant, J. R., Cheesman, M. R., and Butt, J. N. (2008) Spectroelectrochemical characterization of a pentaheme cytochrome in solution and as electrocatalytically active films on nanocrystalline metal-oxide electrodes. *J. Am. Chem. Soc.* **130,** 8588–8589

43. Kabsch, W. (2010) XDS. *Acta Crystallogr. D Biol. Crystallogr.* **66,** 125–132

44. Evans, P. R. (2011) An introduction to data reduction: space-group determination, scaling and intensity statistics. *Acta Crystallogr. D Biol. Crystallogr.* **67,** 282–292

45. Evans, P. (2006) Scaling and assessment of data quality. *Acta Crystallogr. D Biol. Crystallogr.* **62,** 72–82

46. Evans, P. R., and Murshudov, G. N. (2013) How good are my data and what is the resolution? *Acta Crystallogr. D Biol. Crystallogr.* **69,** 1204–1214

47. Vonrhein, C., Flensburg, C., Keller, P., Sharff, A., Smart, O., Paciorek, W., Womack, T., and Bricogne, G. (2011) Data processing and analysis with the autoPROC toolbox. *Acta Crystallogr. D Biol. Crystallogr.* **67,** 293–302

48. Vonrhein, C., Blanc, E., Roversi, P., and Bricogne, G. (2007) Automated structure solution with autoSHARP. *Methods Mol. Biol.* **364,** 215–230

49. de la Fortelle, E., and Bricogne, G. (1997) Maximum-likelihood heavy-atom parameter refinement for multiple isomorphous replacement and multiwavelength anomalous diffraction methods. *Methods Enzymol.* **276,** 472–494

50. Emsley, P., Lohkamp, B., Scott, W. G., and Cowtan, K. (2010) Features and development of Coot. *Acta Crystallogr. D Biol. Crystallogr.* **66,** 486–501

51. Blanc, E., Roversi, P., Vonrhein, C., Flensburg, C., Lea, S. M., and Bricogne, G. (2004) Refinement of severely incomplete structures with maximum likelihood in BUSTER-TNT. *Acta Crystallogr. D Biol. Crystallogr.* **60,** 2210–2221

52. Afonine, P. V., Grosse-Kunstleve, R. W., Echols, N., Headd, J. J., Moriarty, N. W., Mustyakimov, M., Terwilliger, T. C., Urzhumtsev, A., Zwart, P. H., and Adams, P. D. (2012) Towards automated crystallographic structure refinement with phenix.refine. *Acta Crystallogr. D Biol. Crystallogr.* **68,** 352–367

53. Lovell, S. C., Davis, I. W., Arendall, W. B., 3rd., de Bakker, P. I., Word, J. M., Prisant, M. G., Richardson, J. S., and Richardson, D. C. (2003) Structure validation by Cα geometry: ϕ,ψ and Cβ deviation. *Proteins* **50,** 437–450

54. Chen, V. B., Arendall, W. B., 3rd, Headd J. J., Keedy, D. A., Immormino, R. M., Kapral, G. J., Murray, L. W., Richardson, J. S., and Richardson, D. C. (2010) MolProbity: all-atom structure validation for macromolecular crystallography. *Acta Crystallogr. D Biol. Crystallogr.* **66,** 12–21

55. Delano, W. L. (2002) *The PyMOL Molecular Graphics System*, version 1.7.2.1, DeLano Scientific, San Carlos, CA

56. Hanahan, D. (1983) Studies on transformation of *Escherichia coli* with plasmids. *J. Mol. Biol.* **166,** 557–580

57. Karplus, P. A., and Diederichs, K. (2012) Linking crystallographic model and data quality. *Science* **336,** 1030–1033